# Three-dimensional structure of recombinant type 1 inositol 1,4,5-trisphosphate receptor

Francis Wolfram, Edward Morris, Colin W Taylor

# Three-dimensional structure of recombinant type 1 inositol 1,4,5-trisphosphate receptor

Francis WOLFRAM[*], Edward MORRIS[†] and Colin W. TAYLOR[*1]
[*]Department of Pharmacology, University of Cambridge, Tennis Court Road, Cambridge, CB2 1PD, U.K., and [†]Section of Structural Biology, Institute of Cancer Research, Chester Beatty Laboratories, London, SW3 6JB, U.K.

[1]To whom correspondence should be addressed (email cwt1000@cam.ac.uk).

Page heading: 3D structure of $IP_3R$

## SYNOPSIS

Inositol 1,4,5-trisphosphate receptors ($IP_3R$) are the intracellular channels that mediate release of $Ca^{2+}$ from the endoplasmic reticulum in response to the many stimuli that evoke $IP_3$ formation. We characterized and purified type 1 $IP_3R$ heterologously expressed in Sf9 cells, and used the purified $IP_3R1$ to determine its three-dimensional structure by electron microscopy and single particle analysis. Recombinant $IP_3R1$ has four-fold symmetry with overall dimensions of about 19.5 x 19.5 x 17.5 $nm^3$. It comprises a small domain, which is likely to include the pore, linked by slender bridges to a large cytoplasmic domain with four petal-like regions. Our structures of recombinant $IP_3R1$ and native cerebellar $IP_3R$ have similar appearances and dimensions. The only notable difference is the absence of a central stigma-like domain from the cytoplasmic region of recombinant $IP_3R1$. The first structure of a recombinant $IP_3R$ is an important step towards developing 3D structures of $IP_3R$ that better contribute to understanding the structural basis of $IP_3R$ activation.

Key words: $Ca^{2+}$ channel, inositol 1,4,5-trisphosphate receptor ($IP_3R$), electron microscopy (EM), single particle analysis (SPA)

Abbreviations used: CLM, cytosol-like medium; DDM, dodecyl maltoside; ECFP, enhanced cyan fluorescent protein; EM, electron microscopy; ER, endoplasmic reticulum; $IP_3R$, inositol 1,4,5-trisphosphate receptor; PBM, phosphate-buffered medium; RyR, ryanodine receptor; SPA, single particle analysis; TEM, Tris/EDTA medium.

## INTRODUCTION

Cytosolic $Ca^{2+}$ signals regulate diverse cellular activities and most of these signals arise from regulated opening of $Ca^{2+}$-permeable channels. Inositol 1,4,5-trisphosphate receptors ($IP_3R$) are the most widely expressed of these channels [1]. Most $IP_3R$ are expressed in membranes of the endoplasmic reticulum, but they are present also in the plasma membrane of some cells [2], in the nuclear envelope [3], the Golgi apparatus [4] and perhaps also in secretory vesicles [5]. Three vertebrate genes encode closely related subunits of $IP_3R$, each comprising ~2700 amino acid residues. The functional $IP_3R$ is a homo- or hetero-tetrameric assembly of these subunits [6-8]. Each subunit has a single $IP_3$-binding site, the $IP_3$-binding core (residues 224-604), which comprises two domains forming a clam-like structure that encloses a positively charged pocket to which $IP_3$ binds [9]. The N-terminal of the $IP_3R$ (residues 1-223), the suppressor domain, is the only other region of the $IP_3R$ for which a high-resolution structure is available [10]. The head of its hammer-like structure forms a β-trefoil, while the handle comprises a helix-turn-helix motif [10]. Although the structural basis of $IP_3R$ activation remains poorly understood, it is clear that the suppressor domain provides an essential link between $IP_3$ binding to the $IP_3$-binding core and opening of the pore [11, 12]. Furthermore, the N-terminal of ryanodine receptors (RyR), another major family of intracellular $Ca^{2+}$ channels, has a structure almost indistinguishable from that of the suppressor domain of $IP_3R1$ [13], suggesting that both families of intracellular $Ca^{2+}$ channels may share similar gating mechanisms. For both RyR and $IP_3R$ receptors, the $Ca^{2+}$-permeable pore of the channel is formed by the last pair of the six transmembrane helices of each subunit together with the luminal loop that links them. Intermediate resolution structures of RyR, derived from single particle analysis [14, 15], together with sequence alignments [16, 17] and mutagenesis [2, 18] of both RyR [16, 17] and $IP_3R$ [2, 18, 19] are consistent with the idea that the pore of both channels has a structure broadly similar to that of $K^+$ channels [20], with each pair of transmembrane helices cradling an intervening pore helix and selectivity filter. A direct interaction between the suppressor domain and the cytosolic helix that links the fourth and fifth transmembrane domains may mediate gating of $IP_3R$ [11, 12].

High-resolution structures of the complete $IP_3R$ are ultimately required if the structural basis of its activation is to be fully resolved. To date, five intermediate-resolution (~30 Å) structures of $IP_3R1$ purified from cerebellum have been determined using electron microscopy (EM) and single particle analysis (SPA) [21-25]. These structures differ in their details, but they all show a four-fold symmetry and have two distinct regions: a large cytoplasmic domain and a small domain, which is assumed to include the channel region [26]. The first 3D structure to be published had the shape of an uneven dumbbell with a height of 17 nm, and with four arms radiating from the large cytoplasmic domain [22]. We presented a structure reminiscent of a flower, in which the stalk represents the channel domain, and the cytoplasmic regions are represented by the petals and stigma with overall dimensions of ~18x18x18 $nm^3$ [23]. Serysheva *et al.* described the structure of $IP_3R$ as a large cytoplasmic pinwheel with a smaller square-shaped transmembrane domain [27]; its overall dimensions were ~25x25x19 $nm^3$. Hamada *et al.* compared the 3D structures with and without $Ca^{2+}$ and suggested that $Ca^{2+}$ caused $IP_3R$ to switch from a mushroom-like (~19x19x16 $nm^3$) to a windmill-like shape (~22x22x18 $nm^3$), with the head of the mushroom and the wings of the

windmill representing cytosolic domains [21]. The most recent structure resembles a heavily fenestrated hot-air balloon with dimensions of ~17x17x23 $nm^3$ [25]. In the seven to eight years since publication of the first 3D structures of native $IP_3R$ [22, 23, 27, 28], there has been no significant progress towards the higher resolution structures that are required if the structures are contribute further to an understanding of the workings of $IP_3R$.

One approach, with considerable potential to accelerate progress, is to extend EM and SPA analyses of the 3D structure from native $IP_3R$ to recombinant proteins. The benefits might include simplified purification procedures (using tagged $IP_3R$), isolation of more homogenous protein samples than are likely to be present in native tissues, and the opportunity to introduce tags identifiable by EM to allow mapping of primary sequence to the 3D structure. Similar approaches applied to RyR [29-32] have allowed our understanding of its 3D structure to progress well beyond that of $IP_3R$ [33]. Here, we use EM and SPA to establish the first 3D structure of recombinant $IP_3R1$ heterologously expressed in insect Sf9 cells.

## EXPERIMENTAL

### Materials

Foetal bovine serum, primers, fungizone, gentamicin and BSA were from Sigma. ATP and complete protease inhibitor cocktail were from Roche. Dodecyl maltoside (DDM) was from Calbiochem. Restriction enzymes and most molecular biology reagents were from New England Biolabs. [$^3$H]-$IP_3$ (18 Ci/mmol) was from PerkinElmer Life Sciences, and $IP_3$ was from Alexis Biochemicals (Nottingham, U.K.). PreScission protease and the HiTrap Q FF and Superose 6 10/300 GL columns were from GE Healthcare. Mag-fluo-4AM and Sf-900 II SFM medium were from Invitrogen. Other materials were from Sigma, Fisher Scientific or the sources specified in the text or earlier publications [12, 34].

### Expression of $IP_3R1$ in Sf9 cells

A pENTR1A vector encoding $IP_3R1$ N-terminally tagged with ECFP (ECFP-$IP_3R1$) was prepared from two existing pENTR1A vectors containing full-length rat $IP_3R1$ (GenBank: GQ233032.1) and another containing an ECFP-tagged N-terminal of $IP_3R1$ (residues 1-604) by ligation after digestion with NheI and KpnI. The product provided the template from which PCR was used to engineer a C-terminal biotinylation sequence and Prescission-cleavage site (Figure 1A). The reverse primer (5'-TGCATCTCGAGTTATTCGTGCCATTCTATTTTTTGTGCTTCAAAGATG TCGTTGAGTCCGGGCCCCTGGAACAGAACTTCCAGGGCTGGCTGCTGTG GGTTGACATTCATGTG-3') introduced the PreScission cleavage site and biotinylation sequence (Figure 1A). The forward primer (5'-ATGCAGAATTCGGATCCTGTACAACATGAGGCCCAAG-3', corresponding to bases (underlined) 6326-51 of $IP_3R1$) used a unique BstBI site near the 3' end of the open reading frame. The PCR product and ECFP-$IP_3R1$ plasmid were digested with BstBI and Xho1 and ligated to give a pENTR1A

plasmid encoding the tagged $IP_3R1$ shown in Figure 1A. This $IP_3R1$ construct was then transferred into artificial baculovirus DNA (BaculoDirect Linear DNA, Invitrogen) to create recombinant baculovirus DNA. High-titre viral stocks were prepared and the titre determined by end-point dilution [35]. The sequence of the final construct was verified by DNA sequencing.

Sf9 cells were grown in Sf-900 II SFM medium supplemented with 10% foetal bovine serum, 2% fungizone and 1% gentamicin at pH 6.2 in flasks for virus production, and in spinner flasks (stirred at 70 r.p.m.) or shaking bottles (at 135 r.p.m.) for protein expression. Cultures were maintained at 27°C in a humid environment, and passaged every 7 days or when the density exceeded $2x10^6$ cells/ml. For protein expression, Sf9 cells were infected with 10 virus particles per cell (MOI = 10) and harvested after 60 h.

**Purification of $IP_3R1$ from Sf9 cells**

All procedures were performed at 4°C, with incubations mixed by gentle rotation at 15 r.p.m. Infected cells ($3.2x10^9$) were harvested by centrifugation (700x*g*, 5 min), washed with Tris-EDTA medium (TEM: 50 mM Tris, 1 mM EDTA, pH 8.3, and protease inhibitor cocktail) and centrifuged (700x*g*, 5 min). The pellet was suspended in TEM, homogenized with an Ultra Turrax (9500 r.p.m., 2 x 10 strokes) and then with a glass homogenizer (60 strokes), centrifuged (900x*g*, 10 min), and the supernatant was then centrifuged (150,000x*g*, 1 h). The pellet was suspended in TEM (7 ml) and biotinylated by incubation (12-16 h) with D-biotin (100 µM) and biotin-protein ligase (BirA, 9 µg in a final volume 10 ml) according to the manufacturer's instructions (Avidity, Aurora, CO, USA). Membranes were recovered by centrifugation (150,000x*g*, 1 h).

Biotinylated membranes (16 mg total protein/ml) were solubilized in phosphate-buffered medium (PBM: 100 mM $Na_2HPO_4/NaH_2PO_4$, 1 mM ETDA, 5% glycerol, 150 mM NaCl, pH 8, protease inhibitor cocktail and 1% DDM). The yield (~40%) after solubilization is lower than we and others have obtained using Triton-X-100, but DDM is more widely used for solubilization of proteins for structural studies and the background signals in EM were much lower with DDM than with Triton-X-100. After 4 h, the supernatant was recovered after centrifugation (150,000x*g*, 1 h) and incubated (1 h) with streptavidin-agarose beads (Invitrogen, 2 mg protein/100 µl beads). The beads (100 µl) were washed twice with PBM and then resuspended in PreScission medium (100 µl) (PrM: 50 mM Tris, 150 mM NaCl, 1 mM EDTA, 1 mM DTT, 0.2% DDM, pH 7) containing PreScission protease (4 units/100µl beads). After incubation for 12 h, the supernatant was collected by centrifugation (650x*g*, 5 min) and applied to a HiTrap Q FF anion-exchange column, which was then washed (100 ml, 1 ml/min) with ion-exchange medium (50 mM Tris, 150 mM NaCl, 1 mM EDTA, 1 mM DTT, 5% glycerol, 0.02% DDM, pH 8.3). A linear gradient (150-500 mM NaCl in the same medium) was used to elute fractions of 0.5 ml, and the peak fractions (numbers 17-25) were pooled and concentrated to 0.5 ml with a Vivaspin-2 MWCO 30000 centrifugal concentrator (Sartorius). The concentrated sample was applied to a Superose 6 10/300 GL gel-filtration column and fractions (0.5 ml) were eluted with ion-exchange medium (0.5 ml/min). Fractions 21-22 were pooled and used for electron microscopy.

Samples were analysed using pre-cast SDS/PAGE mini-gels (Invitrogen), and by immunoblotting using the iblot system (Invitrogen) with a rabbit anti-peptide antiserum (1:1000) to the C-terminal of $IP_3R1$ [12]. Anti-rabbit, horseradish peroxidase-conjugated secondary antibody (AbCam, 1:5000) and Super Signal West Pico chemiluminescence reagent (Pierce) were used to detect immunoreactivity. The bands were quantified using GeneTools (Syngene). Protein gels were silver-stained using GelCode SilverSNAP II Stain Kit according to the manufacturer's instructions (Pierce).

### $IP_3$-evoked $Ca^{2+}$ release from intracellular stores

The free [$Ca^{2+}$] within the ER was recorded using a low-affinity luminal $Ca^{2+}$ indicator, Mag-fluo4, and a FlexStation plate-reader (MDS Analytical Technologies) [34]. Sf9 cells (~$2x10^6$/ml) were incubated (1 h, 20°C) with Mag-fluo4AM (20 µM) in HEPES-buffered medium (135 mM NaCl, 5.9 mM KCl, 11.6 mM HEPES, 1.5 mM $CaCl_2$, 11.5 mM glucose, 1.2 mM $MgCl_2$, pH 7.3) containing BSA (1 mg/ml) and Pluronic F127 (0.4 mg/ml). The cells were then resuspended in $Ca^{2+}$-free CLM containing saponin (10 µg/ml). Cytosol-like medium (CLM) had the following composition: 20 mM NaCl, 140 mM KCl, 2 mM $MgCl_2$, 1 mM EGTA, 375 µM $CaCl_2$ (free [$Ca^{2+}$] ~200nM), 20 mM PIPES, pH 7. After ~10 min at 37°C the permeabilized cells were washed (650x*g*, 3 min), resuspended in $Mg^{2+}$-free CLM with carbonyl cyanide p-trifluoromethoxyphenylhydraozone (FCCP, 10 µM), distributed into 96-well plates ($6x10^5$ or $2x10^5$ cells in 50 µl/well, for uninfected and infected cells, respectively) and centrifuged (1000x*g*, 3 min). After addition of MgATP (1.5 mM), the intracellular stores loaded to steady-state with $Ca^{2+}$, and after 150 s $IP_3$ was added with thapsigargin (1 µM); the latter to inhibit further $Ca^{2+}$ uptake. $IP_3$-evoked $Ca^{2+}$ release is expressed as a fraction of the ATP-dependent $Ca^{2+}$ uptake. Concentration-effect relationships were fitted to a Hill equation using non-linear curve-fitting (GraphPad Prism, version 5).

### [$^3$H] $IP_3$ binding

Equilibrium-competition binding assays were performed at 4°C in TEM (500 µl) containing [$^3$H]-$IP_3$ (1.5 nM), membranes (~30 µg) or purified $IP_3R$ (~0.7 µg), and appropriate concentrations of $IP_3$. After 5 min, during which equilibrium was attained, incubations were terminated by addition of cold TEM (500 µl) containing polyethylene glycol (PEG) 8000 (30%) and γ-globulin (20 µl of 25 mg/ml), mixed, incubated on ice for 5 min and then centrifuged (20,000x*g*, 5 min). The pellet was rinsed with TEM containing 15% PEG 8000 (2 x 500 µl), and then resuspended to allow its radioactivity to be determined by liquid scintillation counting. Results were fitted to a Hill equation using GraphPad Prism from which the $IC_{50}$ and $K_D$ were determined.

### Electron microscopy and image analysis

Purified $IP_3R1$ was loaded onto glow-discharged carbon-coated copper grids and negatively stained with 2% uranyl acetate. Micrographs were collected on a Tecnai

T-12 electron microscope in low-dose mode (20 electrons/Å$^2$) at a calibrated magnification of 41125, at 120 kV with ~700 nm defocus. The quality of the micrographs was assessed using an optical diffractometer. Only micrographs with circular and isotropic diffraction rings (Thon rings) consistent with a resolution of at least 20 Å within the first ring were used for further processing. Micrographs were digitized using a Nikon Coolscan 9000ED at a step size of 6.35 µm. Scanned micrographs were then converted for processing using IMAGIC programs [36] and 3x3 pixel areas were averaged, resulting in a final pixel size of 0.45 nm. The particles were selected with a box size of 100x100 pixels using the BOXER tool of the EMAN package [37]. IMAGIC [36] was used for all other image processing, except the multi-reference alignment routine for which SPIDER [38] was used. In the first multi-reference alignment and first angular assignment, our previously published $IP_3R$ structure [23], filtered to 54 Å, was used as a reference. The resolution of the 3D reconstruction was determined using the half-bit criterion.

## RESULTS AND DISCUSSION

### Expression, purification and characterization of recombinant $IP_3R1$

After optimization of methods, the outcome of which is described in the Experimental section, we established that infection of Sf9 cells with the tagged $IP_3R1$ construct shown in Figure 1A allowed expression of functional $IP_3R$ at a level considerably exceeding that of endogenous $IP_3R$. Immunoblotting confirmed expression of $IP_3R1$ of appropriate size (~ 300 kDa, see below) in the infected cells. After permeabilization, control and infected cells were each able to accumulate $Ca^{2+}$ after addition of ATP. $IP_3$ caused a barely resolvable $Ca^{2+}$ release from the control cells (maximal $Ca^{2+}$ release, 7 ± 1%; $EC_{50}$, 0.50 ± 0.05 µM; Hill coefficient, 0.9 ± 0.17), but caused a very much larger release from the infected cells (maximal $Ca^{2+}$ release, 47 ± 2%; $EC_{50}$, 1.6 ± 0.41 µM; Hill coefficient, 1.1 ± 0.17) (Figure 1B). In equilibrium-competition assays with [$^3$H]-$IP_3$ using membranes prepared from infected Sf9 cells, $IP_3$ bound with high affinity ($K_D$, 10.49 ± 1.06 nM, Hill coefficient, 0.80 ± 0.08) and the density of the sites ($B_{max}$) was 10.6 ± 0.8 pmol/mg protein (Figure 1C). The affinity of the tagged $IP_3R1$ expressed in Sf9 cells is similar to that determined under the same conditions for native $IP_3R1$ in cerebellar membranes [12] and of untagged $IP_3R1$ expressed in Sf9 cells [23, 39, 40], and the level of expression is ~40-times higher than that of native $IP_3R$ in Sf9 cells [40].

After biotinylation and solubilization (~40% yield), recombinant $IP_3R1$ was purified using streptavidin and then cleavage by PreScission protease (~50% yield), anion-exchange (~16% yield) and size-exclusion chromatography (~70% yield) (see Experimental section). Calibration of the final chromatography step suggested an oligomeric size for the purified $IP_3R$ of ~1.56 MDa, which is consistent with the predicted size of a tetramer of CFP-tagged $IP_3R$ subunits (4 x 339 kDa) associated with DDM (Supplementary Figure S1). The final product migrated as a single band of appropriate size after SDS-PAGE and silver-staining (Figure 2A) or immunoblotting with an $IP_3R1$-selective antiserum (Figure 2B). The $K_D$ of the purified $IP_3R$ for $IP_3$ was 7.65 ± 0.69 nM, Hill coefficient 1.1 ± 0.09 (Figure 2C) and the final specific activity of the sites was 0.25 ± 0.02 nmol/mg protein (their concentration was 24 µg $IP_3R$/ml). EM micrographs of purified

$IP_3R1$ showed particles of the expected size (~20 nm) with their 4-fold symmetry clearly apparent in several profiles (Figure 2D).

These results establish that we have successfully expressed functional $IP_3R1$ at high levels in Sf9 cells and purified them under conditions that allow their structure to be analysed by EM and SPA.

### 3D structure of recombinant $IP_3R1$

The final data set included 7064 particles selected from scanned micrographs. Particles were picked only if they were separated from others and had a size appropriate for an $IP_3R$ (~20 nm). The centred, but otherwise unaligned, particles were subject to multivariate statistical analysis, which yielded 69 eigenimages; the first 10 are shown in Figure 3A. A four-fold symmetry is clearly visible in eigenimages 7 and 8, and a three-fold symmetry is visible in eigenimages 3 and 4. The apparent three-fold symmetry may reflect a side view of the $IP_3R$, which published structures have suggested may be approximately triangular [23, 28]. Much of the data comprises these side views or near side views, with only a fraction of the unaligned data showing four-fold symmetry. The two-fold symmetry in eigenimages 5 and 6 is probably caused by particles that correspond to slightly tilted top or bottom views. Because the $IP_3R$ is tetrameric [26, 41] (Supplementary Figure S1) and all previous EM analyses established a four-fold symmetry [21-25], we applied C4 symmetry to the later stages of our 3D reconstruction.

Class averages of the $IP_3R$ were calculated after reference-free alignment using IMAGIC and then refined using the SPIDER alignment routine using class averages of the initial reference-free alignment (Figure 3B). Figure 3C shows the class averages obtained using native $IP_3R$ [23] as a reference. For the 3D reconstruction, recombinant $IP_3R$ particles were aligned using the filtered native $IP_3R$ structure [23] as a reference in the first iteration; these are similar to the reference-free class averages (Figure 3B). Well-preserved classes with good signal-to-noise ratios were selected and back-projected to produce 3D maps used for further refinement of the classes. The class averages of each iteration cycle were used to obtain a 3D reconstruction that was then used as a reference for the subsequent alignment. The 3D reconstruction was stable after the third iteration. The fast stabilization of the analysis probably arises from our use of a refined structure of the $IP_3R$ [23] as an initial reference.

The final 3D reconstruction contained 22 class averages with a good signal-to-noise ratio (Figures 3D-F) and a wide distribution of Euler angles (Supplementary Figure S2). The resolution, measured using the half-bit criterion of the Fourier shell correlation, was about 40 Å (Supplementary Figure S3). The 3D volume was contoured to accommodate a molecular mass of the recombinant $IP_3R1$ of 1.3 MDa assuming a protein density of 844 Da/nm$^3$. Figure 4A shows the structure of the recombinant $IP_3R$ as sections (each 0.45 nm thick) cut along the symmetry axis and Figure 4B shows four characteristic views of the final 3D reconstruction. The overall dimensions of the 3D structure are ~19.5x19.5x17.5 nm. It comprises a large cytoplasmic region (~19.5x19.5x10 nm$^3$) consisting of four petal-like domains (each ~10.6 nm wide) each connected to a smaller stalk-like channel region (~13.2x13.2x7.5 nm$^3$). This region tapers towards the luminal side to a width of ~7.4 nm (Figures 4A and B).

**Comparison of the structures of native and recombinant $IP_3R$ and RyR**

The 3D structure of recombinant $IP_3R1$, which is likely to be in a closed state, resembles the flower model of the native $IP_3R1$ [23] (Figure 4C), but without the central stigma. The overall dimensions of the two structures are also similar: ~18x18x18 $nm^3$ for native $IP_3R1$, and ~19.5x19.5x17.5 $nm^3$ for recombinant $IP_3R1$ (Figures 4B and C). The cytoplasmic region of each structure is ~11 nm tall and both have a putative channel region that tapers towards the luminal side to a width of ~7 nm. The only substantial difference between the two structures is the absence of a central stigma-like domain from the large cytoplasmic region of recombinant $IP_3R1$ (compare Figures 4Bi and Ci). It is unlikely that this results from inappropriate assembly of the tetrameric $IP_3R$ because the recombinant protein was functional and bound $IP_3$ with appropriate affinity (Figures 1B and C). It may be that the N-terminal ECFP tag stabilized a different closed conformation of the $IP_3R$, or the central stigma may represent an accessory protein [42] that is not present in the heterologous expression system. The 3D structure of a native $IP_3R1$ in a closed state from another group [21] and our structure of recombinant $IP_3R1$ have similar overall dimensions (19x19x16 $nm^3$) and similarly sized channel domains (11x11x5.2 $nm^3$), and both lack a central stigma. However, the four cytoplasmic petal-like regions of our structure are discrete (Figure 4Biii), but they are linked by slender bridges in the native structure [21]. A possible explanation is that the threshold set for the native model (1.7 MDa) is larger than the actual size of native $IP_3R$ (1.2 MDa), leading to inclusion of more density. The pinwheel structure of the native $IP_3R$ [27] has slightly larger dimensions (~25x25x19 $nm^3$), but it shares the four petal-like features of the recombinant $IP_3R$ structure, although their links with the channel region are both more substantial and more centrally placed than in our structure (Figure 4B). The two remaining structures of native $IP_3R$ [22, 25] have similar dimensions to published structures of native $IP_3R$ and to our structure of recombinant $IP_3R1$, but neither has obvious petal-like domains or a stalk-like channel domain.

RyR and $IP_3R$ are relatives that share many structural and functional features, although $IP_3R$ are only half the size of RyR. Both are cation channels with relatively weak selectivity for bivalent over monovalent cations ($P_{Ba}/P_K$ ~ 7), although $IP_3R$ have lesser single channel conductance than RyR [43, 44]. The dimensions and tapering square profile of the channel region of RyR (~11.5x11.5x6 $nm^3$) [15] are similar to that of recombinant $IP_3R1$ (13.2x13.2x7.5 $nm^3$) (Figure 4B). We note also that the large cytoplasmic region of RyR, like that of recombinant $IP_3R1$, has a large central cavity rather than a stigma (Figure 4B).

We have provided the first 3D structure of a recombinant $IP_3R$ at a resolution of ~40Å. The dimensions of our structure and its essential features are similar to the shared structural features of $IP_3R$ purified from native sources (Figure 4). This establishes the utility of recombinant $IP_3R$ and EM and single particle analyses for further elaboration of the structural determinants of $IP_3R$ behaviour.

This work was supported by the Wellcome Trust (CWT) [085295], the Institute of Cancer Research (EM) and by a studentship to FW from the Newton Trust, Cambridge. We thank Dr Paula da Fonseca for advice and assistance with EM and SPA analyses.

## REFERENCES


1 Taylor, C. W., Genazzani, A. A. and Morris, S. A. (1999) Expression of inositol trisphosphate receptors. Cell Calcium **26**, 237-251

2 Dellis, O., Dedos, S., Tovey, S. C., Rahman, T.-U.-., Dubel, S. J. and Taylor, C. W. (2006) $Ca^{2+}$ entry through plasma membrane $IP_3$ receptors. Science **313**, 229-233

3 Stehno-Bittel, L., Lückhoff, A. and Clapham, D. E. (1995) Calcium release from the nucleus by $InsP_3$ receptor channels. Neuron **14**, 163-167

4 Pinton, P., Pozzan, T. and Rizzuto, R. (1998) The Golgi apparatus is an inositol 1,4,5-trisphosphate-sensitive $Ca^{2+}$ store, with functional properties distinct from those of the endoplasmic reticulum. EMBO J. **17**, 5298-5308

5 Gerasimenko, J. V., Lur, G., Sherwood, M. W., Ebisui, E., Tepikin, A. V., Mikoshiba, K., Gerasimenko, O. V. and Petersen, O. H. (2009) Pancreatic protease activation by alcohol metabolite depends on $Ca^{2+}$ release via acid store $IP_3$ receptors. Proc. Natl. Acad. Sci. USA **106**, 10758-10763

6 Supattapone, S., Worley, P. F., Baraban, J. M. and Snyder, S. H. (1988) Solubilization, purification, and characterization of an inositol trisphosphate receptor. J. Biol. Chem. **263**, 1530-1534

7 Chadwick, C. C., Saito, A. and Fleischer, S. (1990) Isolation and characterization of the inositol trisphosphate receptor from smooth muscle. Proc. Natl. Acad. Sci. USA **87**, 2132-2136

8 Furuichi, T., Yoshikawa, S., Miyawaki, A., Wada, K., Maeda, M. and Mikoshiba, K. (1989) Primary structure and functional expression of the inositol 1,4,5-trisphosphate-binding protein $P_{400}$. Nature **342**, 32-38

9 Bosanac, I., Alattia, J.-R., Mal, T. K., Chan, J., Talarico, S., Tong, F. K., Tong, K. I., Yoshikawa, F., Furuichi, T., Iwai, M., Michikawa, T., Mikoshiba, K. and Ikura, M. (2002) Structure of the inositol 1,4,5-trisphosphate receptor binding core in complex with its ligand. Nature **420**, 696-700

10 Bosanac, I., Yamazaki, H., Matsu-ura, T., Michikawa, M., Mikoshiba, K. and Ikura, M. (2005) Crystal structure of the ligand binding suppressor domain of type 1 inositol 1,4,5-trisphosphate receptor. Mol. Cell **17**, 193-203

11 Schug, Z. T. and Joseph, S. K. (2006) The role of the S4-S5 linker and C-terminal tail in inositol 1,4,5-trisphosphate receptor function. J. Biol. Chem. **281**, 24431-24440

12 Rossi, A. M., Riley, A. M., Tovey, S. C., Rahman, T., Dellis, O., Taylor, E. J. A., Veresov, V. G., Potter, B. V. L. and Taylor, C. W. (2009) Synthetic partial agonists reveal key steps in $IP_3$ receptor activation. Nat. Chem. Biol. **5**, 631-639

13 Amador, F. J., Liu, S., Ishiyama, N., Plevin, M. J., Wilson, A., Maclennan, D. H. and Ikura, M. (2009) Crystal structure of type I ryanodine receptor amino-terminal b-trefoil domain reveals a disease-associated mutation "hot spot" loop. Proc. Natl. Acad. Sci. USA **106**, 11040-11044

14 Ludtke, S. J., Serysheva, I. I., Hamilton, S. L. and Chiu, W. (2005) The pore structure of the closed RYR1 channel. Struct. **13**, 1203-1211

15 Samso, M., Wagenknecht, T. and Allen, P. D. (2005) Internal structure and visualization of transmembrane domains of the RyR1calcium release channel by cryo-EM. Nat. Struct. Mol. Biol. **6**, 539-544

16 Ramachandran, S., Serohijos, A. W., Xu, L., Meissner, G. and Dokholyan, N. V. (2009) A structural model of the pore-forming region of the skeletal

muscle ryanodine receptor (RyR1). PLoS Computational Biology **5**, e1000367

17 Balshaw, D., Gao, L. and Meissner, G. (1999) Luminal loop of the ryanodine receptor: A pore-forming segment? Proc. Natl. Acad. Sci. USA **96**, 3345-3347

18 Schug, Z. T., da Fonseca, P. C., Bhanumathy, C. D., Wagner, L., 2nd, Zhang, X., Bailey, B., Morris, E. P., Yule, D. I. and Joseph, S. K. (2008) Molecular characterization of the inositol 1,4,5-trisphosphate receptor pore-forming segment. J. Biol. Chem. **283**, 2939-2948

19 Ramos-Franco, J., Galvan, D., Mignery, G. A. and Fill, M. (1999) Location of the permeation pathway in the recombinant type-1 inositol 1,4,5-trisphosphate receptor. J. Gen. Physiol. **114**, 243-250

20 MacKinnon, R. (2004) Potassium channels and the atomic basis of selective ion conduction (Nobel Lecture). Angew. Chem. Int. Edn. Engl. **43**, 4265-4277

21 Hamada, K., Terauchi, A. and Mikoshiba, K. (2003) Three-dimensional rearrangements with inositol 1,4,5-trisphosphate receptor by calcium. J. Biol. Chem. **278**, 52881-52889

22 Jiang, Q.-X., Thrower, E. C., Chester, D. W., Ehrlich, B. E. and Sigworth, F. J. (2002) Three-dimensional structure of the type 1 inositol 1,4,5-trisphosphate receptor at 24 Å resolution. EMBO J. **21**, 3575-3581

23 da Fonseca, P. C. A., Morris, S. A., Nerou, E. P., Taylor, C. W. and Morris, E. P. (2003) Domain organisation of the type 1 inositol 1,4,5-trisphosphate receptor as revealed by single-particle analysis. Proc. Natl. Acad. Sci. USA **100**, 3936-3941

24 Serysheva, II, Bare, D. J., Ludtke, S. J., Kettlun, C. S., Chiu, W. and Mignery, G. A. (2003) Structure of the type 1 inositol 1,4,5-trisphosphate receptor revealed by electron cryomicroscopy. J Biol Chem **278**, 21319-21322

25 Sato, C., Hamada, K., Ogura, T., Miyazawa, A., Iwasaki, K., Hiroaki, Y., Tani, K., Terauchi, A., Fujiyoshi, Y. and Mikoshiba, K. (2004) Inositol 1,4,5-trisphosphate receptor contains multiple cavities and L-shaped ligand-binding domains. J. Mol. Biol. **336**, 155-164

26 Taylor, C. W., da Fonseca, P. C. A. and Morris, E. P. (2004) $IP_3$ receptors: the search for structure. Trends Biochem. Sci. **29**, 210-219

27 Serysheva, I. I., Bare, D. J., Ludtke, S. J., Kettlun, C. S., Chiu, W. and Mignery, G. A. (2003) Structure of the type 1 inositol 1,4,5-trisphosphate receptor revealed by cryomicroscopy. J. Biol. Chem. **278**, 21319-21322

28 Hamada, K. and Mikoshiba, K. (2002) Two-state conformational changes in inositol 1,4,5-trisphosphate receptor regulated by calcium. J. Biol. Chem. **277**, 21115-21118

29 Jones, P. P., Meng, X., Xiao, B., Cai, S., Bolstad, J., Wagenknecht, T., Liu, Z. and Chen, S. R. (2008) Localization of PKA phosphorylation site, $Ser^{2030}$, in the three-dimensional structure of cardiac ryanodine receptor. Biochem. J. **410**, 261-270

30 Wang, R., Chen, W., Cai, S., Zhang, J., Bolstad, J., Wagenknecht, T., Liu, Z. and Chen, S. R. (2007) Localization of an $NH_2$-terminal disease-causing mutation hot spot to the "clamp" region in the three-dimensional structure of the cardiac ryanodine receptor. J. Biol. Chem. **282**, 17785-17793

31 Liu, Z., Zhang, J., Li, P., Chen, S. R. W. and Wagenknecht, T. (2002) Three-dimensional reconstruction of the recombinant type 2 ryanodine receptor and localization of its divergent region 1. J. Biol. Chem. **277**, 46712-46719

32 Liu, X., Zhang, J., Sharma, M. R., Li, P., Chen, S. R. W. and Wagenknecht, T. (2001) Three-dimensional reconstruction of the recombinant type 3 ryanodine receptor and localization of its amino terminus. Proc. Natl. Acad. Sci. USA **98**, 6104-6109

33 Hamilton, S. L. and Serysheva, I. I. (2009) Ryanodine receptor structure: progress and challenges. J Biol Chem **284**, 4047-4051

34 Tovey, S. C., Sun, Y. and Taylor, C. W. (2006) Rapid functional assays of intracellular $Ca^{2+}$ channels. Nat. Protocol. **1**, 258-262

35 O'Reilly, D. R., Miller, L. K. and Lucklow, V. A. (1994) Baculovirus Expression Vectors. Oxford University Press, Oxford

36 van Heel, M., Harauz, G., Orlova, E. V., Schmidt, R. and Schatz, M. (1996) A new generation of the IMAGIC image processing system. J. Struct. Biol. **116**, 17-24

37 Ludtke, S. J., Baldwin, P. R. and Chiu, W. (1999) EMAN: semiautomated software for high-resolution single-particle reconstructions. J. Struct. Biol. **128**, 82-97

38 Frank, J., Radermacher, M., Penczek, P., Zhu, J., Li, Y., Ladjadj, M. and Leith, A. (1996) SPIDER and WEB: processing and visualization of images in 3D electron microscopy and related fields. J. Struct. Biol. **116**, 190-199

39 Nerou, E. P., Riley, A. M., Potter, B. V. L. and Taylor, C. W. (2001) Selective recognition of inositol phosphates by subtypes of inositol trisphosphate receptor. Biochem. J. **355**, 59-69

40 Cardy, T. J. A., Traynor, D. and Taylor, C. W. (1997) Differential regulation of types 1 and 3 inositol trisphosphate receptors by cytosolic $Ca^{2+}$. Biochem. J. **328**, 785-793

41 Foskett, J. K., White, C., Cheung, K. H. and Mak, D. O. (2007) Inositol trisphosphate receptor $Ca^{2+}$ release channels. Physiol. Rev. **87**, 593-658

42 Patterson, R. L., Boehning, D. and Snyder, S. H. (2004) Inositol 1,4,5-trisphosphate receptors as signal integrators. Annu. Rev. Biochem. **73**, 437-465

43 Rahman, T. and Taylor, C. W. (2009) Dynamic regulation of $IP_3$ receptor clustering and activity by $IP_3$. Channels **3**, 336-332

44 Williams, A. J., West, D. J. and Sitsapesan, R. (2001) Light at the end of the $Ca^{2+}$-release channel tunnel: structures and mechanisms involved in ion translocation in ryanodine receptor channels. Quart. Rev. Biophys. **34**, 61-104

**Figure 1 Recombinant $IP_3R1$ is functional**

(**A**) The recombinant $IP_3R1$ used has an N-terminal ECFP tag, a PreScission protease cleavage site (Pr) and the biotinylation sequene (Biotin). (**B**) $IP_3$-evoked $Ca^{2+}$ release from permeabilized Sf9 cells with or without expression of recombinant $IP_3R1$. (**C**) Specific binding of [$^3$H]-$IP_3$ (1.5 nM) in the presence of the indicated concentrations of $IP_3$ to membranes prepared from Sf9 cells expressing recombinant $IP_3R1$. Results (C and D) are means ± S.E.M (n = 3).

**Figure 2 Purification of recombinant $IP_3R$**

(**A**, **B**) Silver-stained gel (**A**, 0.12 µg protein/lane) and immunoblot with an $IP_3R1$-specific antiserum (**B**, 0.12 µg protein/lane) of purified recombinant $IP_3R1$ from fractions 20-24 of the gel-filtration step. $M_r$ markers (kDa) are shown. Results are typical of at least 5 similar analyses. (**C**) Specific binding of [$^3$H]-$IP_3$ (1.5 nM) in the presence of the indicated concentrations of $IP_3$ to purified recombinant $IP_3R1$ (means ± S.E.M, n = 3). (**D**) EM micrographs of purified recombinant $IP_3R1$ highlighting particles (arrows) with the expected size of tetrameric $IP_3R$ (~20 nm diameter). Scale bar = 70 nm.

**Figure 3 Image analysis of $IP_3R$ particles**

(**A**) Eigenimages of the unaligned data set. Eigenimage 1 shows the sum of all images. Eigenimages 3 and 4 show approximate three-fold symmetry. Eigenimages 5 and 6 show approximate two-fold symmetry. Eigenimages 7 and 8 show four-fold symmetry. (**B**) Class averages obtained independently after two iterative alignments (reference-free classes) (**C**) Similar class averages obtained after three iterative alignment using the filtered 3D structure of native $IP_3R$ [23] as a reference for the first alignment. (**D**) Class averages used for the final 3D reconstruction. (**E**) Re-projections of the final 3D reconstruction corresponding to the class averages shown in D. (**F**) Surface views of the final 3D reconstruction in the same orientations as the class averages. Scale bars (**A**-**F**) = 20 nm.

**Figure 4 Structure of recombinant $IP_3R1$**

(**A**) Each section (1-40) is 0.45 nm thick and viewed along the symmetry axis starting from the cytoplasmic end (1) to the end likely to be within the ER lumen (40). Scale bar = 10 nm. (**B**) Surface views of the 3D reconstruction of recombinant $IP_3R1$ viewed from the cytosol (i), from the lumen of the ER (ii) and two views in cross-section (iii and iv). (**C**) Views similar to those shown in B, but for native cerebellar $IP_3R$ [23]. Scale bars (B and C) = 20 nm.

Biochemical Journal Immediate Publication. Published on 08 Apr 2010 as manuscript BJ20100143



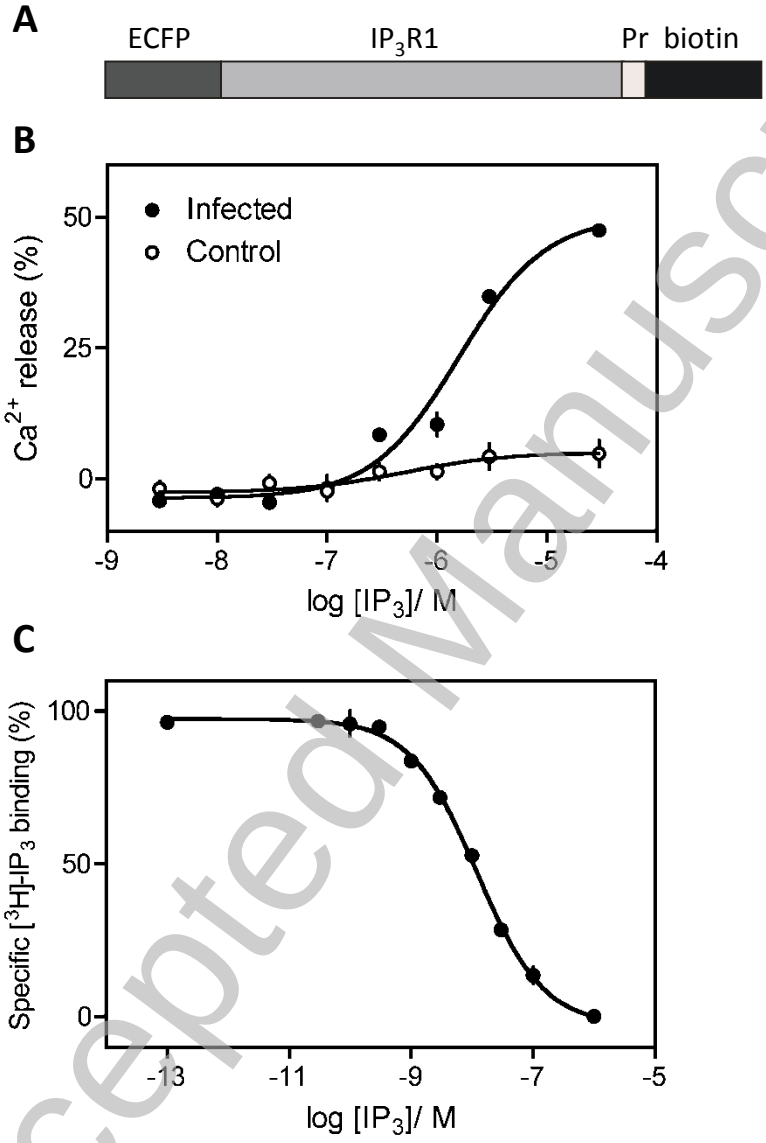

Biochemical Journal Immediate Publication. Published on 08 Apr 2010 as manuscript BJ20100143



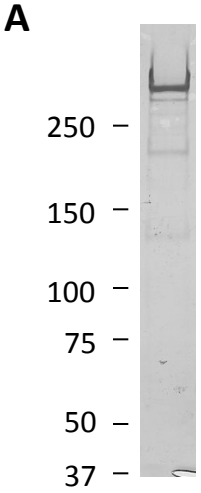


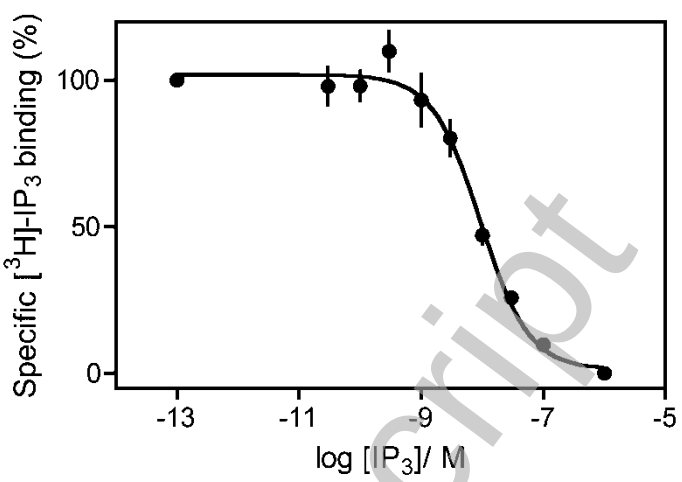


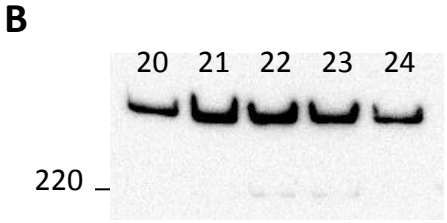


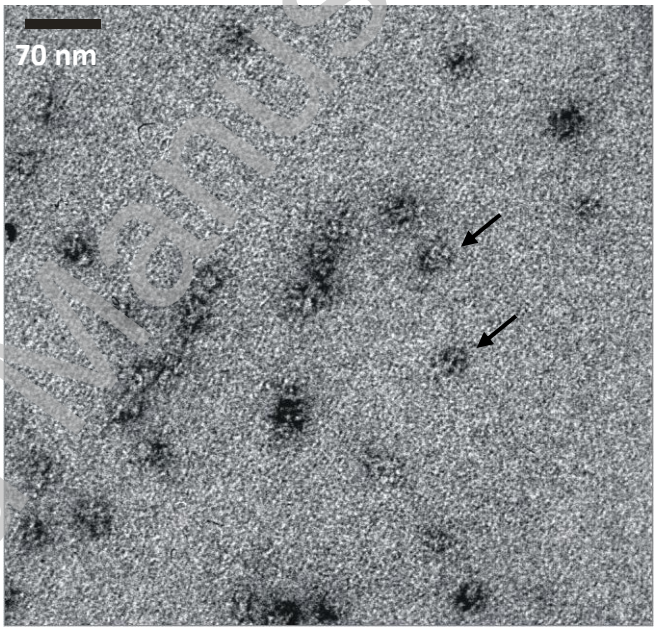

Biochemical Journal Immediate Publication. Published on 08 Apr 2010 as manuscript BJ20100143